Journal of Sound and Vibration (1997) **204**(3), 421–437

THE DYNAMICS OF AN ANNULAR PIEZOELECTRIC MOTOR STATOR

J. R. Friend and D. S. Stutts

Department of Mechanical and Aerospace Engineering and Engineering Mechanics, 1870 *Miner Circle*, *University of Missouri-Rolla*, *Rolla*, *MO* 65409–0050, *U.S.A.*

(*Received* 24 *August* 1995, *and in final form* 25 *October* 1996)

The development of piezoelectric motors has spurred an interest in the vibration characteristics of plates laminated with piezoelectric materials. In particular, this paper details the study of an annular plate composed of one stainless steel lamina and either one or two piezoelectric laminae, a common configuration for piezoelectric motors. The stainless steel layer has teeth milled into the top surface for improved motor behavior. The motion of the teeth is an important characteristic of the motor's performance and is described in detail in this paper. An analytical technique is developed that determines the vibration of the laminate given the input into the piezoelectric layers, and predicts the resulting motion of the teeth.

1. INTRODUCTION

Piezoelectric motors were developed in the early 1980's in response to the need for a lightweight, high-torque, and low-speed motor for fractional horsepower applications. Although the original inventor of the piezoelectric motor remains somewhat in question (many believe H. V. Barth [1] is responsible for the original design), there is no argument about who is responsible for the subsequent development of piezoelectric motor systems. Kumada [2, 3], Kumada *et al*. [4], Sashida [5], Sashida and Kenjo [6], Ueha and Tomikawa [7], and many other Japanese researchers have developed high performance piezoelectric motors for a variety of applications. While piezoelectric motor design continues in Japan and to a lesser extent in the United States and Germany, the kinematics of the motors has received scant attention.

Hagedorn and Wallashek have demonstrated a simple model for the free vibration of a stator disk [8] and an improved model, using the finite difference and Ritz methods, for the free vibration of a disk with non-uniform thickness [9]. However, forcing due to the piezeoelectric elements and the laminated nature of the stator are ignored in their studies. Including these factors into the model makes it more difficult to avoid finite element analysis, and, indeed, Maeno *et al*. [12] studied a ring motor including two-body contact mechanics using a finite element analysis program. Bogy and Maeno [13] examined the motor again with contact mechanics and fluid interaction using a combination of analytical and finite element analysis techniques.

Most laminated structures are modelled as a collection of layers with specific material properties. Several approaches to modelling the laminate are possible; classical lamination theory [14, 15], first order and higher order shear deformation theories with or without rotary inertia [16, 17], and a relatively unique and complex procedure by Reddy and Nosier [18] and Nosier *et al*. [19] are representative of common solution techniques. Tzou *et al*. has developed general laminated composite deep-shell equations [20–22] specifically for

0022–460X/97/280421 + 17 $25.00/0/sv960944

piezoelectrically forced structures. However, all of these methods are limited in their capability to model asymmetric laminated structures with closed-form solutions. With the exception of classical lamination theory and a few cases with the first order shear deformation theory, the problem to be solved always requires finite element analysis. While finite element analysis (FEA) is indispensable for many applications, particularly with complex geometries, it is inconvenient for system design. Each design iteration requires a new finite element mesh to be generated and a new numerical solution to be obtained. This process, known as FEA parametric optimization, is computationally expensive, and it provides a compelling reason to seek analytical solutions.

Approaching the problem with the requirement that all solutions must be of closed-form has its own difficulties, however. There is no assurance, other than experimental verification, that the solution will be accurate after making the necessary approximations. Finite element analysis is avoided by using judicious approximations that retain the behavior of the laminated structure and the teeth. The class of piezoelectric motors modelled are based on the thin annular plate as shown in Figure 1. The analysis presented here is applicable to stator geometries from a solid circular plate ($b = 0$) to an annular ring ($b/a \geqslant 0{\cdot}9$) where shear deformation and rotary inertia are negligible. The modelling approach described here represents an enhancement of the current modelling literature by predicting steady state stator motion directly from the electric potentials applied to the piezoelectric laminas, accounting for the asymmetric laminated structure in an approximate sense, and modelling the kinematics of the stator teeth. The ability to predict the motion of the stator teeth is essential for subsequent modelling of the interaction between the stator and rotor which is required to predict motor performance.

2. ANALYSIS

The linear and quasistatic piezoelectric stress equations for a solid are

$$\bar{\mathbf{D}} = \varepsilon^{\mathrm{T}} \cdot \mathbf{E} + \mathbf{e} : \mathbf{S}, \qquad \bar{\mathbf{T}} = -\mathbf{e} \cdot \mathbf{E} + \mathbf{c}^{E} : \mathbf{S}. \tag{1}$$

The double dot indicates an inner product over two indices of the tensors (a list of symbols is provided in the nomenclature at the end of this paper). For this application (and for most others), the electrical field travels through the piezoelectric material at much higher speeds than the strain field—fast enough to assume that from the perspective of the mechanical motion of the plate, the electrical fields in the piezoelactric laminas change instantaneously. In other words, the motion of the piezoelectric laminates is *quasistatic*. This relatively general form is difficult to work with, but by assuming the stress tensor is symmetric, the equation may be simplified. Contracting the tensor notation as in Auld [23] by applying the symmetric stress tensor assumptions, equations (1) simplifies to

$$\bar{D}_i = \varepsilon_{ij}^{S} E_j + e_{iJ} S_J, \qquad \bar{T}_I = -e_{Ij} E_j + c_{IJ}^{E} S_J. \tag{2}$$

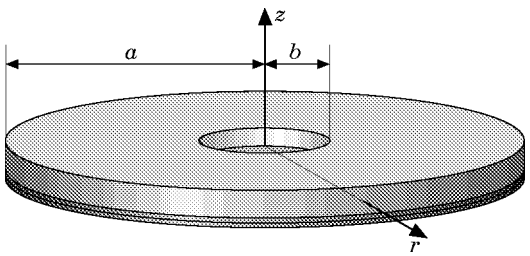

Figure 1. Thin annular plate geometry.

In particular, the stress due to the electric field in the piezoelectric laminas is

$$T_I = -e_{Ij}E_j. \tag{3}$$

The stress-strain relationship in equation (2) will be taken into account in the equation for the transverse motion of the plate below.

3. FREE VIBRATION OF AN ANNULAR PLATE

The behavior of the stator as it freely vibrates is needed for finding the forced behavior of the stator through modal expansion. The stator plate is free of loading on both its inner and outer diameters, and is pinned at the nodal circle as shown in Figure 2 to eliminate rigid body modes. The stator shown in Figure 2 is designed for operation in the (1, 4) vibration mode—one radial node, and four azimuthal wavelengths.

Note that for clarity, in the rest of this paper, references to the three principal co-ordinate directions will use numbers for primary quantities such as displacement, voltage, and material properties, and letters to denote differentiation, and for derived quantities such as moment and shear. Hence, the correspondence is $(1, 2, 3) \equiv (r, \theta, z)$.

The equation of transverse motion [24] of the plate neglecting shear deformation and rotary inertia is

$$(D_{11}^{*}\mathbf{\nabla}^4 + \rho h\partial^2/\partial t^2)u_3 = f(r, \theta, t), \tag{4}$$

where $f(r, \theta, t)$ denotes general forcing,

$$\mathbf{\nabla}^4(\,\cdot\,) = [\mathbf{\nabla}^2(\,\cdot\,)]^2 = \left[\frac{\partial^2(\,\cdot\,)}{\partial r^2} + \frac{1}{r}\frac{\partial(\,\cdot\,)}{\partial r} + \frac{1}{r^2}\frac{\partial^2(\,\cdot\,)}{\partial\theta^2}\right]^2 \tag{5}$$

is the biharmonic operator in polar co-ordinates, and the reduced bending stiffness, D_{11}^{*}, of the composite plate [14, 15] is the (1, 1) component of the matrix $\mathbf{D}^*$ given by

$$\mathbf{D}^* = \mathbf{D} - \mathbf{B}\mathbf{A}^{-1}\mathbf{B}. \tag{6}$$

Shear deformation and rotary inertia may not be neglected for plates where the thickness is large compared to either the overall dimensions of the plate or to the wavelength of the highest mode of interest [25]. According to Mindlin [16], if the ratio of the plate thickness to the wavelength exceeds 0·25, shear deformation and rotary inertia need to be included in the analysis.

The components of $\mathbf{A}$, $\mathbf{B}$, and $\mathbf{D}$, respectively, are

$$A_{ij} = \sum_{l=1}^{n} (Q_{ij})_l (z_l - z_{l-1}), \qquad B_{ij} = \frac{1}{2}\sum_{l=1}^{n} (Q_{ij})_l (z_l^2 - z_{l-1}^2), \tag{7, 8}$$

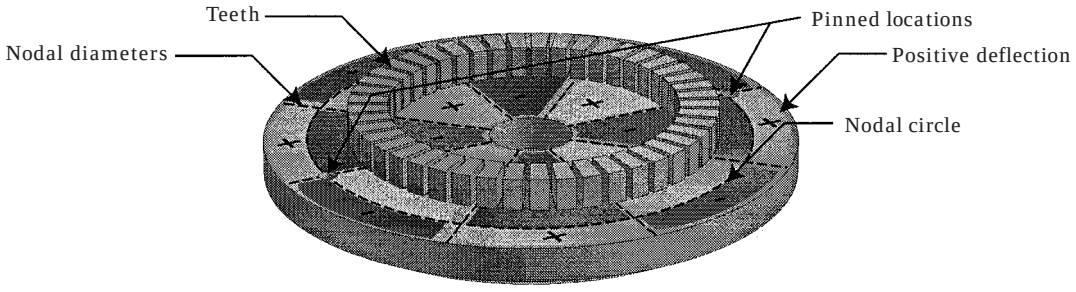

Figure 2. Stator plate with teeth, (1, 4) mode.

and

$$D_{ij} = \frac{1}{3}\sum_{l=1}^{n} (Q_{ij})_l (z_l^3 - z_{l-1}^3). \tag{9}$$

In equations (7–9), the reduced stiffnesses Q_{ij} for the lth layer, assumed to be isotropic in the plane, are given by

$$(Q_{11})_l = (Q_{22})_l = \frac{\mathsf{Y}_l}{1 - \nu_l^2}, \qquad (Q_{12})_l = \frac{\nu_l \mathsf{Y}_l}{1 - \nu_l^2}, \quad \text{and} \quad (Q_{33})_l = G_l. \tag{10}$$

Note that most important polycrystalline piezoeceramic materials are isotropic in a plane normal to the direction of poling, and all polycrystalline piezoceramic materials are completely isotropic when unpoled. The piezoelectric layers in this motor are poled in the transverse direction and so the layers are isotropic in the plane. An alternative form of the reduced stiffnesses Q_{ij} is given by [14]

$$(Q_{ij})_l = c_{ij} - c_{i3}c_{j3}/c_{33}. \tag{11}$$

This form is often more convenient for determining the reduced stiffnesses for piezoelectric materials when the stiffness matrix c_{ij} is given.

Equation (4) is an approximation for the composite nature of the stator ignored in the current literature. The full equations for the general composite plate including asymmetry are extremely complex and are considered to be intractable in closed form. The lamination structure of the stator is indicated in Figure 3 for motors with two piezoelectric layers; motors with only one piezoelectric layer are similar. For the unforced case ($f(r, \theta, t) = 0$), a separable, temporally harmonic solution may be assumed:

$$u_3(r, \theta, t) = U_3(r, \theta)\, \mathrm{e}^{\mathrm{j}\omega t}. \tag{12}$$

Equation (4) becomes

$$(D_{11}^{*}\nabla^4 - \rho h\omega^2)U_3 = 0. \tag{13}$$

By dividing through by D_{11}^{*} and substituting λ^4 for $\rho h\omega^2/D_{11}^{*}$, equation (13) becomes

$$(\nabla^4 - \lambda^4)U_3 = 0, \tag{14}$$

or

$$(\nabla^2 + \lambda^2)(\nabla^2 - \lambda^2)U_3 = 0. \tag{15}$$

This equation has solutions of the same form as the equation

$$(\nabla^2 \pm \lambda^2)U_3 = 0. \tag{16}$$

Separating the spatial variables,

$$U_3(r, \theta) = R(r)F(\theta), \tag{17}$$

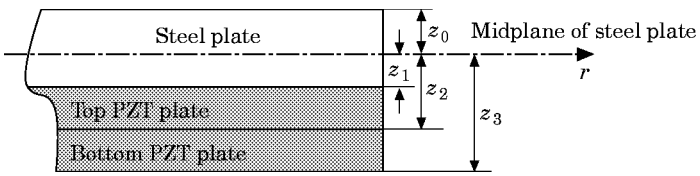

Figure 3. Lamination structure and nomenclature (not to scale).

equation (16) becomes

$$r^2\left[\left(\frac{\mathrm{d}^2R}{\mathrm{d}r^2}=\frac{1}{r}\frac{\mathrm{d}R}{\mathrm{d}r}\right)\frac{1}{R}\pm\lambda^2\right]=-\frac{1}{F}\frac{\mathrm{d}^2F}{\mathrm{d}\theta^2}=n^2 \tag{18}$$

by grouping the r-dependent terms on the left and the θ-dependent terms on the right. Solving, the complete solution for the plate is

$$u_{3mn}(r,\theta,t)=[A_1\mathrm{J}_n(\lambda_{mn}r)+A_2\mathrm{I}_n(\lambda_{mn}r)+A_3\mathrm{Y}_n(\lambda_{mn}r) +A_4\mathrm{K}_n(\lambda_{mn}r)]\cos[n(\theta-\phi_{mn})]\,\mathrm{e}^{\mathrm{j}\omega t} \tag{19}$$

For the piezoelectric motor in this study, the stator plate is annular and is not loaded on either the inner or outer radius with loads as shown in Figure 4, and the piezoelectric layers are assumed to be thin in comparison with the stator plate. The boundary conditions for this configuration with Kirchoff's approximation are

$$M_{rr}=-D_{11}^{*}\left[\frac{\partial^2u_3}{\partial r^2}+\nu\left(\frac{1}{r}\frac{\partial u_3}{\partial r}+\frac{1}{r^2}\frac{\partial^2u_3}{\partial\theta^2}\right)\right]=0 \tag{20}$$

and

$$V_{rz}=-D_{11}^{*}\left[\frac{\partial}{\partial r}\nabla^2u_3+\frac{1-\nu}{r^2}\frac{\partial^2}{\partial\theta^2}\left(\frac{\partial u_3}{\partial r}-\frac{u_3}{r}\right)\right]=0, \tag{21}$$

for both the inner and outer radii of the annular stator plate as suggested by Raju [24]. Other motor configurations can be considered by changing the boundary conditions to any combination of fixed, pinned or free boundaries. The variable M_{rr} is the resultant (mechanical) moment on the inner and outer radial faces of the plate and V_{rz} is the resultant shear at the same locations. The electrode pattern on the PZT plates does not extend all the way to the inner and outer boundaries, so the boundary conditions are purely mechanical. Since the moment and the shear (transverse to the plate) are both zero on the inner and outer boundaries, equations (20) and (21) are set equal to zero. The solution for the plate, equation (19), must be substituted into equations (20) and (21) to give four equations in terms of the parameter λ_{mn} and the four constants A_i:

$$\begin{bmatrix}C_{11}&C_{12}&C_{13}&C_{14}\\C_{21}&C_{22}&C_{23}&C_{24}\\C_{31}&C_{32}&C_{33}&C_{34}\\C_{41}&C_{42}&C_{43}&C_{44}\end{bmatrix}\begin{bmatrix}A_1\\A_2\\A_3\\A_4\end{bmatrix}=0, \tag{22}$$

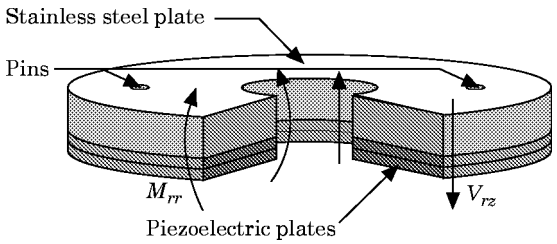

Figure 4. Piezoelectric motor plate (teeth not shown).

where C_{1j} refers to the substitution of equation (19) into the moment equation (20) for the inner radius and collected in terms of A_i. Similarly, C_{2j} refers to the substitution of equation (19) into equation (20) for the outer radius, C_{3j} refers to the substitution of equation (19) into equation (21) for the inner radius, and C_{4j} refers to the substitution of equation (19) into equation (21) for the outer radius. For a useful solution, all of the A_i cannot be zero; this problem becomes an eigenvalue problem for λ_{mn}, which is embedded in the C_{ij}. Taking the determinant of the matrix $[C_{ij}]$ and solving for λ_{mn} will give the resonant frequency of the plate for the (m, n) mode by solving for the resonant frequency ω_{mn} in

$$\omega_{mn} = \lambda_{mn}^2 \sqrt{D_{11}^*/\rho h}. \tag{23}$$

Finding the mode shape for a given (m, n) requires the use of equation (22) again. Assuming that A_4 is unity, the remaining A_i may be found in terms of A_4, which would determine all of the A_i within a constant. Setting $A_4 = 1$ in equation (22) and simplifying gives

$$\begin{bmatrix} C_{11} & C_{12} & C_{13} \\ C_{21} & C_{22} & C_{23} \\ C_{31} & C_{32} & C_{33} \\ C_{41} & C_{42} & C_{43} \end{bmatrix} \begin{Bmatrix} A_1 \\ A_2 \\ A_3 \end{Bmatrix} = \begin{Bmatrix} -C_{14} \\ -C_{24} \\ -C_{34} \\ -C_{44} \end{Bmatrix}, \tag{24}$$

an overdetermined equation. Using only the first three rows of the matrix, the remaining A_i may be found:

$$\begin{Bmatrix} A_1 \\ A_2 \\ A_3 \end{Bmatrix} = \begin{bmatrix} C_{11} & C_{12} & C_{13} \\ C_{21} & C_{22} & C_{23} \\ C_{31} & C_{32} & C_{33} \end{bmatrix}^{-1} \begin{Bmatrix} -C_{14} \\ -C_{24} \\ -C_{34} \end{Bmatrix}. \tag{25}$$

The piezoelectric motor in this study is a flat disk with a constant thickness, but many piezoelectric motors have varying thicknesses to increase their performance characteristics. Hagedorn *et al*. [8, 9] explored the analysis of these types of stators in great detail using the Ritz method, and finite difference analysis. Conway *et al*. [10, 11] found an analytical solution for an annular plate with parabolically varying thickness in the radial direction. Some axisymmetric annular plate based piezoelectric motors have step-wise constantly varying stator thickness, and Hagedorn and Wallashek [8] suggested the use of a multiple domain approach to determine the free vibration in this case.

The multiple domain approach could make it possible to approximately analyze ring motors with a thin support web and with large teeth like the Shinsei motor [5]. The approximation is due to the requirement that the plate be symmetric about the neutral surface; most of the motors like the Shinsei motor are not symmetric about the neutral surface. Generally, an accurate analysis of asymmetric plates requires a numerical approach.

Hagedorn and Wallashek [8] also points out the necessity of accounting for the stator teeth if these are of significant size relative to the overall dimensions of the stator. In this study, the stiffness contribution of the stator teeth is neglected due to their relatively small size (eight teeth per wave length) but the mass contribution of each tooth is lumped into the mass of the stator. These assumptions seem reasonable, and the resulting model predictions agree well with experiment as will be demonstrated below.

4. THE STEADY-STATE FORCED RESPONSE OF THE STATOR

The stators in most piezoelectric motors are forced through bending due to the expansion and contraction of the piezoelectric layers in the stator. The in-plane expansion and contraction of the entire stator is usually negligible in comparison, as is the forcing of the stator from transverse deformation of the piezoelectric layers (due to the $d_{33}E_3$ term).

Once the mode shapes and resonant frequencies of the free–free plate are known, the motion of the forced plate may be determined through modal expansion. During the forced vibration of plates and shells, several different modes may participate simultaneously in different amounts depending on the type of forcing. The amount of participation that each mode offers in response to the external forcing is called the *modal participation factor* for that mode, and it is solely a function of time. The general solution to the transverse vibration of the annular plate is a summation of the plate vibration solution, equation (19), over all of the possible modes of vibration:

$$u_3(r, \theta, t) = \sum_{m=0}^{\infty} \sum_{n=1}^{\infty} \eta_{mn}(t) U_{3mn}(r, \theta). \tag{26}$$

The stator in this motor design is forced primarily through moment forcing from the planar expansion and contraction of the piezoelectric laminas.

From Tzou [26], the equation of motion for the transverse vibration of a deep shell with applied moment forcing M_{ij}^a and transverse forcing T_3 can be written as

$$L_z(M_{ij}) - c_v \dot{u}_3 - \rho h \ddot{u}_3 = -T_3 - L_z(M_{ij}^a) \tag{27}$$

where $L_z(M_{ij})$ is Love's operator in the transverse direction on the moment per unit length induced in the plate, and $L_z(M_{ij}^a)$ is Love's operator on the applied moment per unit length due to the deformation of the piezoelectric laminas. Structural damping in the plate is included here (as equivalent viscous damping) as a part of the general forcing term. The operator $L_z(M_{ij})$ simplifies into the left side of equation (4) and the operator $L_z(M_{ij}^a)$ may be replaced by its definition to give

$$(D_{11}^* \nabla^4 + c_v \dot{u}_3 + \rho h \partial^2/\partial t^2) u_3 = T_3 - L_3(M_{ij}^a) = T_3 + \left(2 \frac{\partial M_{rr}^a}{r \partial r} + \frac{\partial^2 M_{rr}^a}{\partial r^2} - \frac{\partial M_{\theta\theta}^a}{r \partial r} + \frac{\partial^2 M_{\theta\theta}^a}{r^2 \partial \theta^2} \right), \tag{28}$$

where $M_{r\theta}$ and $M_{\theta r}$ are zero since the piezoelectric laminas will not induce the twisting moments $M_{r\theta}$ and $M_{\theta r}$ in the stator [26].

Substituting equation (26) into equation (28) gives

$$\sum_{m=0}^{\infty} \sum_{n=1}^{\infty} (D_{11}^* \eta_{mn} \nabla^4 U_{3mn} + c_v \dot{\eta}_{mn} U_{3mn} + \rho h \ddot{\eta}_{mn} U_{3mn})$$

$$= T_3 + \left(2 \frac{\partial M_{rr}^a}{r \partial r} + \frac{\partial^2 M_{rr}^a}{\partial r^2} - \frac{\partial M_{\theta\theta}^a}{r \partial r} + \frac{\partial^2 M_{\theta\theta}^a}{r^2 \partial \theta^2} \right). \tag{29}$$

From the analysis on the free plate,

$$D_{11}^* \nabla^4 U_{3mn} - \rho h \omega_{mn}^2 U_{3mn} = 0, \tag{30}$$

so equation (29) becomes

$$\sum_{m=0}^{\infty}\sum_{n=1}^{\infty}(\rho h\omega_{mn}^2\eta_{mn}U_{3mn}+c_v\dot{\eta}_{mn}U_{3mn}+\rho h\ddot{\eta}_{mn}U_{3mn}) = T_3+\left(2\frac{\partial M_{rr}^a}{r\partial r}+\frac{\partial^2 M_{rr}^a}{\partial r^2}-\frac{\partial M_{\theta\theta}^a}{r\partial r}+\frac{\partial^2 M_{\theta\theta}^a}{r^2\partial\theta^2}\right). \quad (31)$$

For convenience, the resonant modes of the plate are renumbered to reduce the double subscript (m, n) to the single subscript n; the (1, 0) mode becomes the (1) mode and so on [25]. Multiplying both sides by U_{3k}, where k is necessarily equal to n gives

$$\sum_{n=1}^{\infty}(\rho h\omega_n^2\eta_n+c_v\dot{\eta}_n+\rho h\ddot{\eta}_n)U_{3n}U_{3k}=\left[T_3+\left(2\frac{\partial M_{rr}^a}{r\partial r}+\frac{\partial^2 M_{rr}^a}{\partial r^2}-\frac{\partial M_{\theta\theta}^a}{r\partial r}+\frac{\partial^2 M_{\theta\theta}^a}{r^2\partial\theta^2}\right)\right]U_{3k}. \quad (32)$$

In practice, the induced forcing is usually designed to excite a single mode by ensuring that the forcing closely matches the desired mode, so the complete summation of modes over both n and k collapses into a single summation over n with a given constant k. Integrating both sides over the plate midplane to exploit the orthogonality of the modes gives

$$\int_r\int_\theta\sum_{n=1}^{\infty}(\rho h\omega_n^2\eta_n+c_v\dot{\eta}_n+\rho h\ddot{\eta}_n)U_{3n}U_{3k}r\,\mathrm{d}\theta\,\mathrm{d}r = \int_r\int_\theta\left[T_3+\left(2\frac{\partial M_{rr}^a}{r\partial r}+\frac{\partial^2 M_{rr}^a}{\partial r^2}-\frac{\partial M_{\theta\theta}^a}{r\partial r}+\frac{\partial^2 M_{\theta\theta}^a}{r^2\partial\theta^2}\right)\right]U_{3k}r\,\mathrm{d}\theta\,\mathrm{d}r \quad (33)$$

or

$$\sum_{n=1}^{\infty}(\rho h\omega_n^2\eta_n+c_v\dot{\eta}_n+\rho h\ddot{\eta}_n)\int_r\int_\theta U_{3n}U_{3k}r\,\mathrm{d}\theta\,\mathrm{d}r = \int_r\int_\theta\left[T_3+\left(2\frac{\partial M_{rr}^a}{r\partial r}+\frac{\partial^2 M_{rr}^a}{\partial r^2}-\frac{\partial M_{\theta\theta}^a}{r\partial r}+\frac{\partial^2 M_{\theta\theta}^a}{r^2\partial\theta^2}\right)\right]U_{3k}r\,\mathrm{d}\theta\,\mathrm{d}r. \quad (34)$$

The integrals may move within the infinite sum by assuming that the plate surface is continuous with derivatives that are continuous to the second order (class $\mathscr{C}^2$). Since each mode of plate vibration is orthogonal to every other mode,

$$\int_r\int_\theta U_{3n}U_{3k}r\,\mathrm{d}\theta\,\mathrm{d}r=\left\{\begin{array}{lll}0 & \text{if} & k\neq n\\ \displaystyle\int_r\int_\theta U_{3n}^2 r\,\mathrm{d}\theta\,\mathrm{d}r & \text{if} & k=n\end{array}\right\}. \quad (35)$$

Hence, all the terms in the infinite sum in equation (34) vanish except for the one when $n = k$. A single ordinary differential equation remains to be solved for the modal particpitation factor of mode k:

$$\ddot{\eta}_k+2\zeta_k\omega_k\dot{\eta}_k+\omega_k^2\eta_k=F_k, \quad (36)$$

where

$$F_k = \frac{1}{\rho h N_k} \int_r \int_\theta \left[T_3 + \left(2 \frac{\partial M^a_{rr}}{r \partial r} + \frac{\partial^2 M^a_{rr}}{\partial r^2} - \frac{\partial M^a_{\theta\theta}}{r \partial r} + \frac{\partial^2 M^a_{\theta\theta}}{r^2 \partial \theta^2} \right) \right] U_{3k} r \, \mathrm{d}\theta \, \mathrm{d}r, \tag{37}$$

$$N_k = \int_r \int_\theta U^2_{3k} r \, \mathrm{d}\theta \, \mathrm{d}r, \tag{38}$$

and

$$\zeta_k = c_v / 2 \rho h \omega_k . \tag{39}$$

In the present example, the transverse forcing term is assumed to be neglegible ($T_3 = 0$), but in a more sophisticated model it could be used to account for transverse loading on the stator. As motors are normally used, the transverse forcing term is of much lower order than the piezoelectric forcing, for if too much preload is applied, the PZT elements will become clamped [23].

The steady state harmonic response of the plate vibration is the most important part of the motor's operation, since the transient part lasts only a few milliseconds for most motors. Since the response will be harmonic, the solution for equation (36) is

$$\eta_k = \Lambda_k \, \mathrm{e}^{\mathrm{j}(\omega t - \phi_k)}. \tag{40}$$

Substituting this into equation (36) and solving for Λ_k gives

$$\Lambda_k = \frac{F^*_k}{(\omega_k^2 - \omega^2) + 2\mathrm{j}\zeta_k \omega_k \omega} \, \mathrm{e}^{-\mathrm{j}\phi_k}, \tag{41}$$

where

$$F^*_k = \frac{1}{\rho h N_k} \int_r \int_\theta \left(2 \frac{\partial M^{a*}_{rr}}{r \partial r} + \frac{\partial^2 M^{a*}_{rr}}{\partial r^2} - \frac{\partial M^{a*}_{\theta\theta}}{r \partial r} + \frac{\partial^2 M^{a*}_{\theta\theta}}{r^2 \partial \theta^2} \right) U_{3k} r \, \mathrm{d}\theta \, \mathrm{d}r. \tag{42}$$

The magnitude of the response is

$$|\Lambda_k| = F^*_k / \omega_k^2 \sqrt{[1 - (\omega/\omega_k)^2]^2 + 4\zeta_k^2 (\omega_k/\omega)^2}, \tag{43}$$

and the phase lag angle ϕ_k is

$$\delta_k = \arctan [2\zeta_k (\omega/\omega_k)/(1 - (\omega/\omega_k)^2)]. \tag{44}$$

If there is only one mode being excited in the plate, then only one solution of the modal participation factor is necessary, making the solution process relatively simple.

In equation (42), F^*_k expresses the modal loading on the plate for any fixed point in time on the kth mode. It only depends on the spatial variables r and θ. In a piezoelectric motor, the induced fields in the piezoelectric plate and thus the loading by a single piezoelectric laminate can be assumed to be constant over the area covered by a particular electrode as shown in Figure 5 since, for most applications, the resistance of the electrode is low. In this motor, there is an even number of electrodes that cover the entire surface of the piezoelectric plate with the exception of small gaps between the electrodes to prevent shorting. If all of the electrodes are identical in shape and size, an equation for the applied potential may be determined fairly easily:

$$v_{3,1} = \left\{ \begin{array}{ccl} v_3^* & \text{if} & 4p\pi/\hat{n} \leqslant \theta < \theta_{elect} + 4p\pi/\hat{n} \\ -v_3^* & \text{if} & 4p\pi/\hat{n} + \theta_{elect} + \theta_{gap} \leqslant \theta < 2\theta_{elect} + \theta_{gap} + 4p\pi/\hat{n} \\ 0 & \text{if} & 4p\pi/\hat{n} + \theta_{elect} \leqslant \theta < \theta_{elect} + \theta_{gap} + 4p\pi/\hat{n} \end{array} \right\}, \tag{45}$$

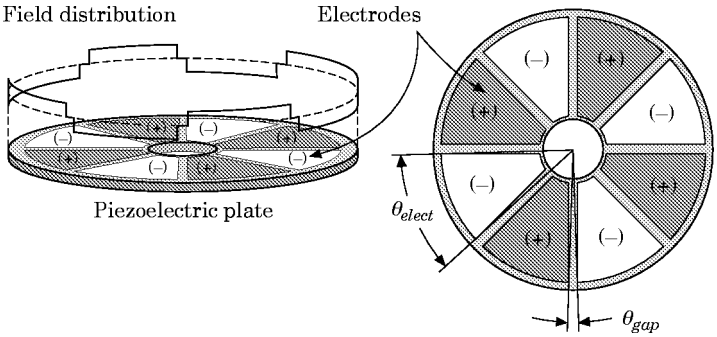

Figure 5. Stepwise electric field distribution.

where v_3^* is the peak potential applied to the piezoelectric lamina, $\hat{n}$ is the number of electrodes, and the index $p \in \{0, 1, \ldots, \hat{n}/2 - 1\}$ selects each electrode pair for each value of p. The angles θ_{elect} and θ_{gap} indicate the angular width of a single electrode and the gap between two electrodes. If a second piezoelectric lamina is present, the potential applied to it may be out of phase with the potential applied to the other piezoelectric layer:

$$v_{3,2} = \left\{ \begin{array}{lll} v_3^* & \text{if} & 4p\pi/\hat{n} \leqslant \theta + \phi_{PZT} < \theta_{elect} + 4p\pi/\hat{n} \\ -v_3^* & \text{if} & 4p\pi/\hat{n} + \theta_{elect} + \theta_{gap} \leqslant \theta + \phi_{PZT} < 2\theta_{elect} + \theta_{gap} + 4p\pi/\hat{n} \\ 0 & \text{if} & 4p\pi/\hat{n} + \theta_{elect} \leqslant \theta + \phi_{PZT} < \theta_{elect} + \theta_{gap} 4p\pi/\hat{n} \end{array} \right\}, \quad (46)$$

where ϕ_{PZT} is the phase angle between the two piezoelectric laminas. This angle between the two layers is necessary to create a traveling wave in many piezoelectric motors. Some motors use only one piezoelectric plate and employ complex electroding patterns to obtain the traveling wave. The equations for the applied voltages for these types of motors are much more lengthy, although they are not any more complex than equations (45) and (46). Notice that, for a motor with two piezoelectric layers, both layers are assumed to have the same peak applied electrical potential and the same thickness. Assuming that the spatial distribution of the electric fields are in this form eliminates the need to determine the electrical and mechanical boundary conditions for the piezoelectric plates and the associated field distribution in them. This assumption also neglects the effect of *piezoelectric stiffening*, the increase in the stiffness of piezoelectric materials when the material is in an open circuit or in a highly resistive circuit. These assumptions are justified since the piezoelectric laminas are relatively thin in comparison with the stator [26].

The moment forcing on the plate due to planar expansion of the piezoelectric plate can be expressed by

$$M_{\theta\theta}^{a*} = \tfrac{1}{2}[e_{32} v_{3,1}](h_{PLATE} + h_{PZT}) \cos(\omega t + \phi_t), \quad (47)$$

illustrated by Figure 6. The analogous expression for the radial moment is

$$M_{rr}^{a*} = \tfrac{1}{2}[e_{31} v_{3,1}](h_{PLATE} + h_{PZT}) \cos(\omega t + \phi_t), \quad (48)$$

These equations give the moments exerted by a single piezoelectric layer with respect to the midplane of the stainless steel layer excited with a temporally harmonic electric field distribution. For two piezoelectric layers, the radial and circumferential moments are

$$M_{rr}^{a*} = \tfrac{1}{2}[e_{31} v_{3,1}](h_{PLATE} + h_{PZT}) \cos(\omega t + \phi_t) + \tfrac{1}{2}[e_{31} v_{3,2}](h_{PLATE} + 3h_{PZT}) \cos(\omega t + \phi_t) \quad (49)$$

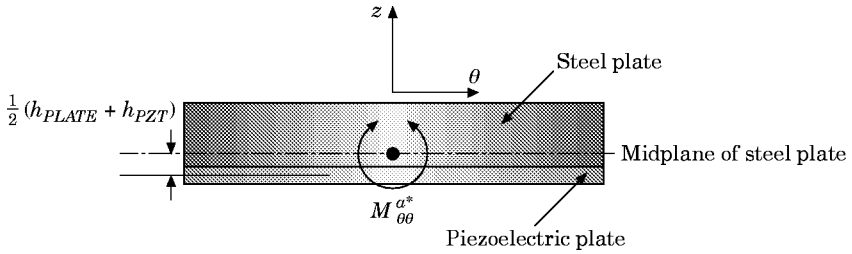

Figure 6. Moment forcing by one piezoelectric plate about radial axis.

and

$$M_{\theta\theta}^{a*} = \tfrac{1}{2}[e_{32}v_{3,1}](h_{PLATE} + h_{PZT})\cos(\omega t + \phi_t) + \tfrac{1}{2}[e_{32}v_{3,2}](h_{PLATE} + 3h_{PZT})\cos(\omega t + \phi_t), \quad (50)$$

illustrated by Figure 7.

5. MOTION OF THE TEETH

From the plate vibration solution,

$$u_3 = u_3(r, \theta, t) = \eta_n(t)U_{3n}(r, \theta) \quad (51)$$

is the solution for a plate vibrating *solely* in the nth mode. A vector from the center of the annular plate at its midplane to a point in the midplane of the deformed plate along an arbitrary radius is given by

$$\mathbf{x} = r\mathbf{e}_r + u_3\mathbf{e}_z. \quad (52)$$

To determine the motion of a tooth on the surface of the plate, a unit vector normal to the surface is needed. Taking the derivative of equation (52) with respect to r (holding time fixed),

$$\partial\mathbf{x}/\partial r = \mathbf{e}_r + (\partial u_3/\partial r)\mathbf{e}_z, \quad (53)$$

and taking the derivative of equation (52) with respect to θ and dividing by r gives

$$\partial\mathbf{x}/r\partial\theta = \mathbf{e}_\theta + (\partial u_3/r\partial\theta)\mathbf{e}_z, \quad (54)$$

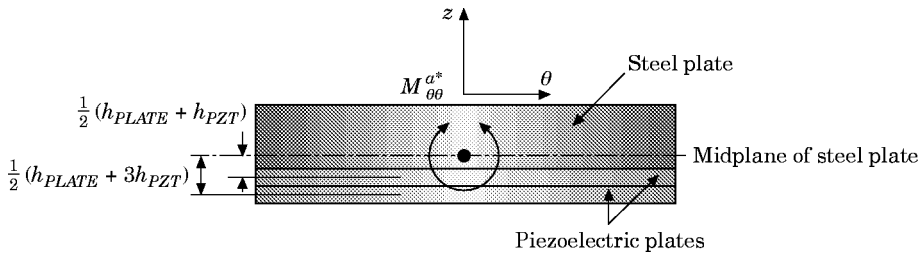

Figure 7. Moment forcing by two piezoelectric plates about radial axis.

two equations which represent tangent vectors along the surface at (r, θ) in the radial and circumferential directions, respectively. Taking the cross-product of these two vectors and normalizing to find the unit normal vector to the surface,

$$\mathbf{N} = \mathbf{T}_r \times \mathbf{T}_\theta = \frac{\partial \mathbf{x}}{\partial r} \times \frac{\partial \mathbf{x}}{r\partial\theta} = \begin{vmatrix} \mathbf{e}_r & \mathbf{e}_\theta & \mathbf{e}_z \\ 1 & 0 & \dfrac{\partial u_3}{\partial r} \\ 0 & 1 & \dfrac{\partial u_3}{r\partial\theta} \end{vmatrix} = -\frac{\partial u_3}{\partial r}\,\mathbf{e}_r - \frac{\partial u_3}{r\partial\theta}\,\mathbf{e}_\theta + \mathbf{e}_z, \tag{55}$$

gives

$$\mathbf{e}_N = \frac{N}{|\mathbf{N}|} = \frac{\mathbf{N}}{\sqrt{1 + (\partial u_3/\partial r)^2 + (\partial u_3/r\partial\theta)^2}}. \tag{56}$$

Then the vector to the end of the tooth has the form

$$\mathbf{x}_T = \mathbf{x} + [h_{TOOTH} \tfrac{1}{2} h_{PLATE}]\mathbf{e}_N \tag{57}$$

for the piezoelectric motor. Fully expanded, equation (57) is

$$\mathbf{x}_T = (r - \overline{h}\partial u_3/\partial r)\mathbf{e}_r - (\overline{h}\partial u_3/r\partial\theta)\mathbf{e}_\theta + (u_3 + \overline{h})\mathbf{e}_z, \tag{58}$$

where $\overline{h}$ is given by

$$\overline{h} = [h_{TOOTH} + \tfrac{1}{2} h_{PLATE}]/\sqrt{1 + (\partial u_3/\partial r)^2 + (\partial u_3/r\partial\theta)^2}. \tag{59}$$

This gives the location of the *center* of the top of each tooth if one knows its location on the plate as shown in Figure 8. Equation (58) effectively transforms the plate vibration solution into a tooth displacement solution for any point (r, θ).

For the piezoelectric motor, the location of the teeth is specified as a part of the design. To make it easier to determine the motion of the teeth, the location of each tooth is based on an index i, its arc-width $(r\theta)_T$, the arc-width of the gap between each tooth $(r\theta)_{gap}$, the location of the inner radius of the teeth $r_{T_{in}}$, and the location of the outer radius of the teeth $r_{T_{out}}$. The location of the center of each tooth is, then,

$$r_T = \tfrac{1}{2}(r_{T_{in}} + r_{T_{out}}), \qquad \theta_T = [(r\theta)_T + (r\theta)_{gap}]/r_T i, \tag{60}$$

where i is the tooth selected. These two equations can be used in equation (58) to describe the motion of those teeth.

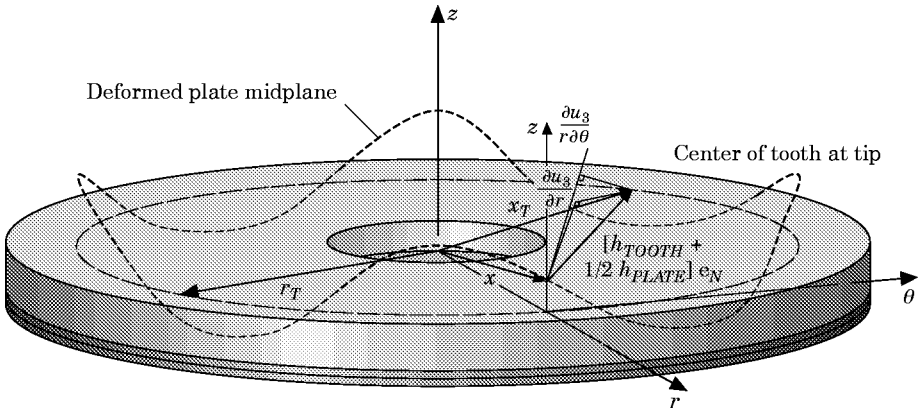

Figure 8. Illustration of tooth kinematics (not to scale).

TABLE 1

Geometric properties of the 17 *mm motor*

Property	Value
Number of teeth	32
Inner radius of plate, a (m)	$1{\cdot}59 \times 10^{-4}$
Outer radius of plate, b (m)	$8{\cdot}48 \times 10^{-3}$
Thickness of stator, h_{PLATE} (m)	$6{\cdot}35 \times 10^{-4}$
Thickness of piezo. plates, h_{PZT} (m)	$1{\cdot}27 \times 10^{-4}$
$r_{T_{in}}$ (m)	$4{\cdot}67 \times 10^{-3}$
$r_{T_{out}}$ (m)	$5{\cdot}61 \times 10^{-3}$
Height of teeth, h_{TOOTH} (m)	$1{\cdot}91 \times 10^{-3}$
θ_T (rad)	0·16144
θ_{gap} (rad)	0·0349
Maximum applied field, E_3^* (V/cm)	1900
Number of electrodes per plate	8
ϕ_{PZT} (rad)	$\pi/8$

6. RESULTS

There are a wide variety of piezoelectric motor designs with a concomitant number of geometric constraints on the analysis of these designs. As an example, a relatively simple motor design invented by researchers at Matsushita, the 17 mm piezoelectric motor, is described here. The 17 mm piezoelectric motor stator is constructed of stainless steel, and the piezoelectric plates are composed of a hard piezoelectric material: PZT-5H. A variety of piezoelectric materials are available for use in the motor, although in practice, only the PZT (lead-zirconium-titanate) class of ceramics is viable for high electric field applications like this one. For this motor, Table 1 provides the geometric data necessary for the analysis. The motor is operated in the (1, 4) mode, causing the stator plate to have four nodal diameters and one nodal circle (see Figure 2). To achieve this mode, each piezoelectric plate has eight electrodes.

Using the free vibration analysis for the Kirchoff annular plate, the prediction of the resonant frequency for the plate of 143 kHz is 6% above the experimentally measured 135 kHz. This indicates that the composite corrections for the stator are accurate and that rotary inertia and shear deformation *for this particular case* are negligible. The piezoelectric plates are electrically excited near the resonant frequency to develop the (1, 4) mode shape. Transverse deflection of the stator reaches 2 μm at its maximum, illustrating how

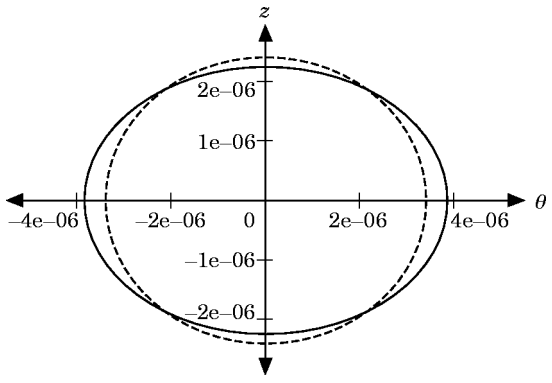

Figure 9. Tooth displacement (m) viewed from the side (dotted line indicates experimental results).

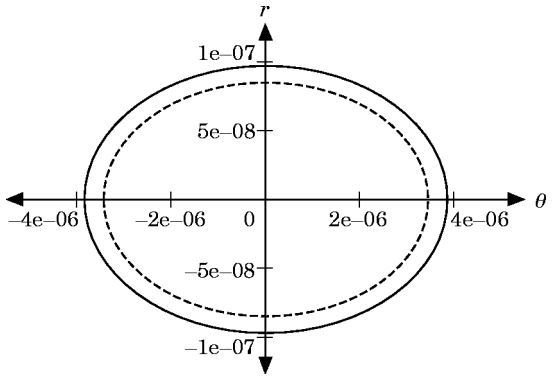

Figure 10. Tooth displacement (m) viewed from the top (dotted line indicates experimental results).

small the deformation of the stator are as the motor operates. This deformation is harmonic in time, and it causes the tips of the stator teeth to generate an elliptical motion as shown in Figures 9 and 10. From the side, the elliptical motion is roughly twice as wide as it is tall, yet the overall motion is minuscule at less than 4 μm. The dotted lines indicate experimental results based upon optical measurements (of maximum and minimum deflection in each direction) taken at a tooth tip. At first glance it would seem that this motion is too small to develop a large-scale motion from the rotor. However, it is important to remember that a tooth will make a complete cycle around the ellipse in only 8×10^{-6} s. Looking from the top, the elliptical motion is mostly azimuthal, as desired. The azimuthal component of the motion acts to rotate the rotor, while the radial component merely causes frictional losses. For this reason, the teeth are placed as close to the azimuthal antinode as possible to ensure that as the plate flexes, the teeth do not bend inward and outward radially.

7. CONCLUSIONS

An analytical model of a composite piezoelectric motor stator with teeth has been described. This model provides three significant contributions to the piezoelectric motor literature: it allows the prediction of steady state stator motion given an applied electrical potential for either one or two piezoelectric plate elements, it accounts for the composite structure of the stator in predicting the natural frequencies and modes, and it predicts the kinematics of the stator teeth. The approach described forms the foundation for rapid design prototyping and subsequent optimization once the model is extended to account for rotor-stator interaction. An example of using the analysis on a piezoelectric motor system is described. The results of the analysis are accurate enough to use the method for design purposes.

Work is currently underway to extend this model to account for the contact mechanics between the rotor and stator, and these results will be presented in a subsequent paper. This extension will allow the prediction of motor performance metrics such as torque and speed. Model predictions can then be compared to experimentally measured performance metrics in a variety of commercially available piezoelectric motors.

REFERENCES

1. H. V. Barth 1973 *IBM Technical Disclosure Bulletin* **16**, 2263.
2. A. Kumada 1987 U.S. Patent 4,642,509, February 10, Ultrasonic motor using bending, longitudinal and torsional vibrations: 10 claims and 14 drawing sheets.

3. A. KUMADA 1989 *U.S. Patent* 4,868,446, *September* 19. Piezoelectric revolving resonator and ultrasonic motor; 10 Claims, 17 Drawing Sheets.
4. A. KUMADA, T. IOCHI and M. OKADA 1991 *U.S. Patent* 5,008,581, *April* 16. Piezoelectric revolving resonator and single-phase ultrasonic motor; 6 Claims, 6 Drawing Sheets.
5. T. SASHIDA 1985 *U.S. Patent* 4,562,374, *December* 31. Motor device utilizing ultrasonic oscillation; 29 Claims, 22 Drawings.
6. T. SASHIDA and T. KENJO 1993 *An Introduction to Ultrasonic Motors*. Oxford: Clarendon Press; p. 242.
7. S UEHA and Y. TOMIKAWA 1993 *Ultrasonic Motors—Theory and Applications*. Oxford: Clarendon Press; p. 297.
8. P. HAGEDORN and J. WALLASHEK 1992 *Journal of Sound and Vibration* **155**, 31–46. Travelling wave ultrasonic motors, part I: working principle and mathematical modeling of the stator.
9. J. WALLASHEK, P. HAGEDORN, and W. KONRAD 1993 *Journal of Sound and Vibration* **168**, 115–122. Travelling wave ultrasonic motors, part II: a numerical method for the flexural vibrations of the stator.
10. H. D. CONWAY, E. C. H. BECKER and J. F. DUBIL 1964 *Journal of Applied Mechanics* **31**, 329–331. Vibration frequencies of tapered bars and circular plates.
11. T. A. LENOX and H. D. CONWAY 1980 *Journal of Sound and Vibration* **31**, 231–339. An exact, closed form, solution for the flexural vibration of a thin annular plate having a parabolic thickness variation.
12. T. MAENO, T. TSUKIMOTO and A. MIYAKE 1990 *7th IEEE International Symposium on Application of Ferroelectrics*, Kangawa, Japan. 535–538. The contact mechanism of an ultrasonic motor.
13. T. MAENO and D. BOGY 1992 *Institute of Electrical and Electronic Transactions on Ultrasonics, Ferroelectrics and Frequency Control* **39**, 675–682. Effect of the hydrodynamic bearing on rotor/stator contact in a ring-type ultrasonic motor.
14. J. E. ASHTON and J. M. WHITNEY 1970 *Theory of Laminated Plates*. Stamford CA: Technomic; p. 153.
15. R. SZILARD 1974 *Theory and Analysis of Plates—Classical and Numerical Methods*. Englewood Cliffs, NJ: Prentice-Hall; p. 724.
16. R. D. MINDLIN 1951 *Journal of Applied Mechanics, Transactions of the ASME, Series E* **73**, 31–38. Influence of rotatory inertia and shear on flexural motions of isotropic, elastic plates.
17. J. N. REDDY 1990 *Journal of Nonlinear Mechanics* **25**, 677–686. A general third-order nonlinear theory of plates with moderate thickness.
18. J. N. REDDY 1990 *Shock and Vibration Digest* **22**, 3–17. A review of refined theories of laminated composite plates.
19. A. NOSIER, R. K. KAPANIA and J. N. REDDY 1993 *American Institute of Aeronautics and Astronautics Journal* **8**, 2335–2346. Free vibration analysis of laminated plates using a layerwise theory.
20. H. S. TZOU and M. GADRE 1990 *Journal of Sound and Vibration* **136**, 477–490. Active vibration isolation and excitation by piezoelectric slab with constant feedback gains.
21. H. S. TZOU 1991 *Journal of Dynamic Systems, Measurement and Control* **113**, 500–505. Distributed modal identification and vibration control of continua: piezoelectric finite element formulation and analysis.
22. H. S. TZOU and J. ZHONG 1992 *Journal of Dynamic Systems, Measurement and Control* **115**, 506–517. Electromechanics and vibrations of piezoelectric shell distributed systems.
23. B. A. AULD 1990 *Acoustic Fields and Waves in Solids*. Malabar, FL: Krieger. Two Volumes; p. 435.
24. P. RAJU 1962 *Journal of the Aeronautical Society of India* **14**, 37–50. Vibrations of annular plates.
25. W. SOEDEL 1993 *Vibrations of Shells and Plates*. New York: Marcel Dekker. Second edition; p. 470.
26. H. S. TZOU 1993 *Piezoelectric Shells—Distributed Sensing and Control of Continua*. Solid Mechanics and Its Applications; Boston: Kluwer; p. 470.

8. NOMENCLATURE

$\mathbf{V}^4 = (\mathbf{V}^2)^2$	Biharmonic operator (see equation (5))
a, b	Inner and outer radii of annular plate, respectively
A_i	Constants ($i = 1, 2, 3, 4$)
$\mathbf{A}, A_{ij}$	Composite plate in-plane stiffness matrix

$\mathbf{B}$, B_{ij}	Composite stiffness coupling matrix
$\mathbf{c}$, c_{IJ}	Material stiffness tensor ($\mathbf{c}^E$ is measured with a constant electric field)
c_v	Equivalent viscous damping in stator
$\mathbf{D}$, D_{ij}	Composite plate bending stiffness matrix
$\mathbf{D}^*$, D_{ij}^*	Reduced composite plate bending stiffness (see Ashton and Whitney [14])
$\bar{\mathbf{D}}$, $\bar{D}_i$	Charge displacement vector
$\mathbf{e}$, e_{Ij}	Piezoelectric stress tensor
$\boldsymbol{\varepsilon}$, ε_{ij}	Permittivity tensor ($\boldsymbol{\varepsilon}^{\mathrm{T}}$ is measured with a constant stress field, $\boldsymbol{\varepsilon}^S$ is measured with a constant strain field)
Y	Young's modulus
$\mathbf{E}$, E_j	Induced electric field tensor
$\mathbf{e}_r$, $\mathbf{e}_\theta$, $\mathbf{e}_z$	Unit vectors along co-ordinates axes
$f(r, \phi, t)$	Forcing on plate
F_k	Modal forcing (F_k^* indicates harmonic forcing)
$F(\theta)$	Azimuthal solution of transverse plate motion
ϕ_k	Phase angle for the kth modal solution of freely vibrating plate
ϕ_{PZT}	Rotation angle between the bottom piezoelectric layer and the top piezoelectric layer
ϕ_t	Phase angle of induced electric field (temporal)
G	Shear modulus
h	Thickness of the stator
h_i	Thickness of lamina i ($i = PLATE, PZT$)
h_{TOOTH}	Height of the teeth measured from the top of the stator
η	Modal participation factor ($0 \leqslant \eta \leqslant 1$)
i, I, j, J	Spatial subscripts ($=1, 2, 3$)
j	Imaginary unit
$\mathbf{J}_n$, $\mathbf{I}_n$	Bessel's original and modified functions of the first kind, respectively
l	Selected layer in the stator
L_3	Love's operator for the transverse vibration of a plate (see [26])
λ	Eigenvalue of characteristic equation of plate
k	Selected mode (after renumbering of modes)
m	Radial mode number (number of circular modal lines)
M_{ij}^a*	Applied moment per unit length (M_{rr}^a*, $M_{\theta\theta}^a$* are applied about the radial and azimuthal directions, respectively)
M_{ij}	Moments per unit length in plate
n	Mode shape number or number of diametral modal lines
$\hat{n}$	Number of electrodes
ν, ν_k	Poisson's ratio
$\mathbf{N}$, $\mathbf{e}_\mathbf{N}$	Vector and unit vector normal to the deformed plate's midplane, respectively
N_k	Modal normalization factor
p	index, $\in\{0, 1, \ldots, \hat{n}/2-1\}$
Q_{ij}	Reduced stiffness matrix (see [14])
ρ	Density of the plate
r	Radial coordinate
$R(r)$	Radial solution of transverse plate motion
$r_{T_{in}}$, $r_{T_{out}}$	Radius to the inner and outer edges of the teeth, respectively
$(r\theta)_T$, $(r\theta)_{gap}$	Arclength of tooth and gap between adjacent teeth, respectively
$\mathbf{S}$, S_J	Strain tensor
t	Time
$\mathbf{T}$, $\bar{T}_I$, T_I	Stress tensor, components, and stress components due to electrical excitation, respectively
T_i	Forcing in the ith direction
$\mathbf{T}_r$, $\mathbf{T}_\theta$	Vectors tangent to midplane surface in radial and azimuthal directions, respectively
θ	Azimuthal coordinate
θ_{elect}	Angular width of one electrode
θ_{gap}	Angular width between two adjacent electrodes
u_3	Transverse displacement (time domain)
U_3	Transverse displacement (frequency domain)
v_3	Electric potential applied transversely across piezoelectric plate ($v_{3,1}$ is applied to top piezoelectric plate, $v_{3,2}$ to bottom plate)
v_3^*	Peak electric potential applied to piezoelectric plate

ω	Circular frequency of applied forcing (rad/s)
ω_k	Resonant circular frequency of kth mode of plate (rad/s)
$\mathbf{x}$	Vector to a point on the midplane of the annular plate from the center at the midplane
$\mathbf{x}_T$	Vector to the end of a tooth from the center of the midplane
Y_n, K_n	Bessel's original and modified functions of the second kind, respectively
z_k	Distance from the midplane of the composite plate to the kth interface ($k = 0$ indicates the top of the plate, $k = 1$ indicates the interface between the stator and the top PZT plate, and so on)
ζ_k	Damping of kth mode of plate